






RESEARCH ARTICLE

Gradient of microstructural damage along the dentato-thalamo-cortical tract in Friedreich ataxia

Sirio Coccozza¹  , Sara Bosticardo², Matteo Battocchio², Louise Corben^{3,4,5}, Martin Delatycki^{3,4,5}, Gary Egan^{6,7}, Nellie Georgiou-Karistianis⁵, Serena Monti⁸, Giuseppe Palma⁹, Chiara Pane¹⁰, Francesco Saccà¹⁰ , Simona Schiavi^{2,11}, Louisa Selvadurai⁵, Mario Tranfa¹ , Alessandro Daducci², Arturo Brunetti¹ & Ian H. Harding^{7,12} 

¹Department of Advanced Biomedical Sciences, University of Naples "Federico II", Naples, Italy

²Department of Computer Science, Diffusion Imaging and Connectivity Estimation (DICE) Lab, University of Verona, Verona, Italy

³Bruce Lefroy Centre for Genetic Health Research, Murdoch Children's Research Institute, Parkville, Victoria, Australia

⁴Department of Pediatrics, University of Melbourne, Parkville, Victoria, Australia

⁵School of Psychological Sciences, The Turner Institute for Brain and Mental Health, Monash University, Clayton, Victoria, Australia

⁶Turner Institute for Brain and Mental Health, School of Psychological Sciences, Monash University, Clayton, Victoria, Australia

⁷Monash Biomedical Imaging, Monash University, Clayton, Victoria, Australia

⁸Institute of Biostructures and Bioimaging, National Research Council, Napoli, Italy

⁹Institute of Nanotechnology, National Research Council, Lecce, Italy

¹⁰Department of Neurosciences Reproductive and Odontostomatological Sciences, University of Naples "Federico II", Naples, Italy

¹¹ASG Superconductors SpA, Genoa, Italy

¹²Department of Neuroscience, Central Clinical School, Monash University, Melbourne, Victoria, Australia

Correspondence

Sirio Coccozza, Department of Advanced Biomedical Sciences, University "Federico II", Via Pansini 5, Naples 80131, Italy. Tel: +390817462569; Fax: +390817463561; E-mail: sirio.coccozza@unina.it

Received: 8 December 2023; Revised: 2 February 2024; Accepted: 29 February 2024

Annals of Clinical and Translational Neurology 2024; 11(7): 1691–1702

doi: 10.1002/acn3.52048

Abstract

Objective: The dentato-thalamo-cortical tract (DTT) is the main cerebellar efferent pathway. Degeneration of the DTT is a core feature of Friedreich ataxia (FRDA). However, it remains unclear whether DTT disruption is spatially specific, with some segments being more impacted than others. This study aimed to investigate microstructural integrity along the DTT in FRDA using a profilometry diffusion MRI (dMRI) approach. **Methods:** MRI data from 45 individuals with FRDA (mean age: 33.2 ± 13.2 , Male/Female: 26/19) and 37 healthy controls (mean age: 36.5 ± 12.7 , Male/Female: 18/19) were included in this cross-sectional multicenter study. A profilometry analysis was performed on dMRI data by first using tractography to define the DTT as the white matter pathway connecting the dentate nucleus to the contralateral motor cortex. The tract was then divided into 100 segments, and dMRI metrics of microstructural integrity (fractional anisotropy, mean diffusivity and radial diffusivity) at each segment were compared between groups. The process was replicated on the arcuate fasciculus for comparison. **Results:** Across all diffusion metrics, the region of the DTT connecting the dentate nucleus and thalamus was more impacted in FRDA than downstream cerebral sections from the thalamus to the cortex. The arcuate fasciculus was minimally impacted. **Interpretation:** Our study further expands the current knowledge about brain involvement in FRDA, showing that microstructural abnormalities within the DTT are weighted to early segments of the tract (i.e., the superior cerebellar peduncle). These findings are consistent with the hypothesis of DTT undergoing anterograde degeneration arising from the dentate nuclei and progressing to the primary motor cortex.

Introduction

Friedreich ataxia (FRDA) is one of the most common inherited ataxias, most frequently caused by a

homozygous GAA triplet-repeat expansion in the first intron of the frataxin gene (*FXN*).¹ The neurological features of FRDA include progressive cerebellar dysfunction with limb and gait ataxia, dysarthria, oculomotor

disturbances, sensory deafferentation, and reduced tendon reflex responses.²

In FRDA, central nervous system pathology primarily impacts the cerebellum and spinal cord. In particular, the dentate nuclei represent a significant site of damage, with significant volume loss coupled with changes in iron concentration.^{3–5} The involvement of the cerebellar cortex is less robust and more variable in people with FRDA.^{6–9} Magnetic resonance imaging (MRI) has identified both macro- and micro-structural changes not only at the level of the spinal cord and cerebellum but also in cerebellar-cerebral pathways, thalamus, and more subtly within the cerebral cortex.^{6,10–12} In particular, widespread brain microstructural changes have been reported in the white matter in individuals with FRDA, with pronounced involvement of the superior and inferior cerebellar peduncles and corticospinal tracts.^{6,9,10}

Magnetic resonance imaging research has provided strong evidence for degeneration of the dentato-thalamo-cortical tract (DTT) in FRDA, a primary efferent pathway of the cerebellum. This includes atrophy, demyelination, and axonal degeneration of the superior cerebellar peduncles (SCP), which form the first section of the DTT.^{10,13} Additionally, changes in functional activation in the cerebral cortex and altered cerebello-cerebral connectivity are evident in people with FRDA in the absence of robust cerebral gray matter changes.^{14–16} These findings support the likelihood of secondary cerebral dysfunction as a consequence of DTT breakdown. However, it remains unclear whether the DTT is impacted along its entire length, or if some subsections are more impacted than others.

The aim of this study was therefore to further map the involvement of DTT in FRDA by taking a spatially targeted approach to understanding whether the tract is uniformly

impacted or, alternatively, whether the abnormalities are spatially distributed. We hypothesized that the pattern of microstructural damage affecting the DTT would be most pronounced in the proximity of the dentate nuclei, with the severity of damage reducing along the tract from the cerebellum to the motor cortex, consistent with current models of anterograde trans-synaptic damage in FRDA.¹⁷

Methods

Subjects

In this cross-sectional multicenter study, 45 individuals with FRDA (26 males, 32.5 ± 14.1 years and 19 females, 34.0 ± 12.1 years) and 37 healthy controls (HC, 18 males, 35.8 ± 12.6 years and 19 females, 37.1 ± 13.1 years) were enrolled. Magnetic resonance imaging data were acquired at three different sites (Site 1: IMAGE-FRDA, Melbourne; Site 2: INFLAM-FRDA, Melbourne; and Site 3: University of Naples “Federico II”, Naples, Italy). A complete list of clinical and demographic information of the entire group, and stratified by per site, is available in Table 1.

All individuals with FRDA received a molecular diagnosis of FRDA with a homozygous expansion of the *FXN* gene, obtained by conventional genetic test with short and long triplet repeat primed polymerase chain reaction. Subjects with any other neurological disorder, or psychiatric conditions, were not included in the study. For all patients, a neurological examination was performed within 1 week of the acquisition of the MRI data, including the Scale for the Assessment and Rating of Ataxia (SARA). Age at onset (AAO), defined as the age when the subject first presented with symptoms of the disease, was also recorded.

The study was ethically approved and governed at each site (Site 1: Monash Health Human Research Ethics

Table 1. Demographic and clinical information.

	Whole group	Site 1	Site 2	Site 3
FRDA	<i>n</i> = 45	<i>n</i> = 13	<i>n</i> = 21	<i>n</i> = 11
(Age, sex—M/F)	33.2 ± 13.2, 26/19	26.7 ± 6.56, 8/5	37.2 ± 13.2, 11/10	33.1 ± 16.6, 7/4
HC	<i>n</i> = 37	<i>n</i> = 9	<i>n</i> = 17	<i>n</i> = 11
(Age, sex—M/F)	36.5 ± 12.7, 18/19	27.9 ± 6.55, 4/5	42.7 ± 12.7, 7/10	33.9 ± 12.2, 7/4
SARA	19.2 (4.0–30.5)	20.5 (8.0–30.0)	22.2 (4.0–30.5)	16.0 (7.0–24.0)
AAO	16.7 ± 7.76	14.5 ± 3.53	19.8 ± 8.72	13.5 ± 7.95
GAA1	593 (118–1200)	558 (280–925)	562 (126–1077)	850 (118–1200)
GAA2	918 (205–1293)	883 (526–1135)	946 (215–1293)	903 (205–1250)

Table showing the demographic and clinical information of the subjects included in this study. Ages and AAO are expressed in years and reported as mean ± standard deviation. SARA and GAA triplets are reported as median (range).

AAO, age at onset; FRDA, Friedreich ataxia; HC, healthy controls; SARA, scale for the assessment and rating of ataxia.

Committee, protocol 13201B, Site 2: Monash University Human Research Ethics Committee, protocol 2017-7810, Site 3: Approval no. 47/15 of the “Carlo Romano” Ethical Committee of “Federico II” University of Naples, Italy). All studies were performed in accordance with the Declaration of Helsinki, with written informed consent obtained from all participants.

MRI data acquisition

All subjects underwent MRI on 3 T Siemens scanners (Siemens, Erlangen, Germany), including a volumetric T1-weighted sequence, a diffusion MRI sequence, and a multi-echo T2* sequence used for quantitative susceptibility mapping (QSM). The acquisition parameters differed between sites (see Supplementary Materials for full acquisition details), but all sites included both an FRDA cohort and an age and sex-matched control group (Table 1), allowing for robust post-processing data harmonization and statistical control procedures (see below).

MRI data analysis

A graphical representation of the main processing steps is provided in Figure 1.

dMRI preprocessing

MRtrix3 v3.0.2 was used to reconstruct the anatomically constrained tractography of the whole brain for all the acquired images.¹⁸ A five-tissue-type segmentation (gray

matter, cortical white matter, sub-cortical gray matter, and cerebrospinal fluid) was first performed on the T1-weighted images. These were then registered to the diffusion space using the FMRIB linear image registration tool with a boundary-based algorithm implemented in FSL v.6.0.4.¹⁹ For Sites 1 and 2, a fiber orientation distributions (FODs) approach was used for each tissue type using the multi-shell multi-tissue algorithm,²⁰ while for Site 3, a single-shell multi-tissue algorithm (<https://3tissue.github.io/>) was used. For each subject, 3 millions streamlines were generated using the iFOD2 algorithm of MRtrix3.²¹ A diffusion tensor model was fit in FSL to generate microstructural maps of fractional anisotropy (FA), mean diffusivity (MD), and radial diffusivity (RD)²² for each dataset. Finally, to account for site differences in data acquisition and processing, and standardize the data for statistical analyses, the calculated DTI maps were harmonized using the ComBat Harmonization algorithm (<https://github.com/Jfortin1/ComBatHarmonization>).²³

Region-of-Interest (ROI) identification

Prior to reconstructing the DTT, we first isolated a set of anatomical ROIs that are way-points along the tract. Masks of the dentate nuclei and red nuclei were manually delineated by a trained rater, blinded to disease status, using the QSM images (see Supplementary Materials for QSM reconstruction methods). The thalamus and precentral gyri were automatically segmented from the T1-weighted images using FreeSurfer v6.0.0 (<http://surfer.nmr.mgh.harvard.edu>).

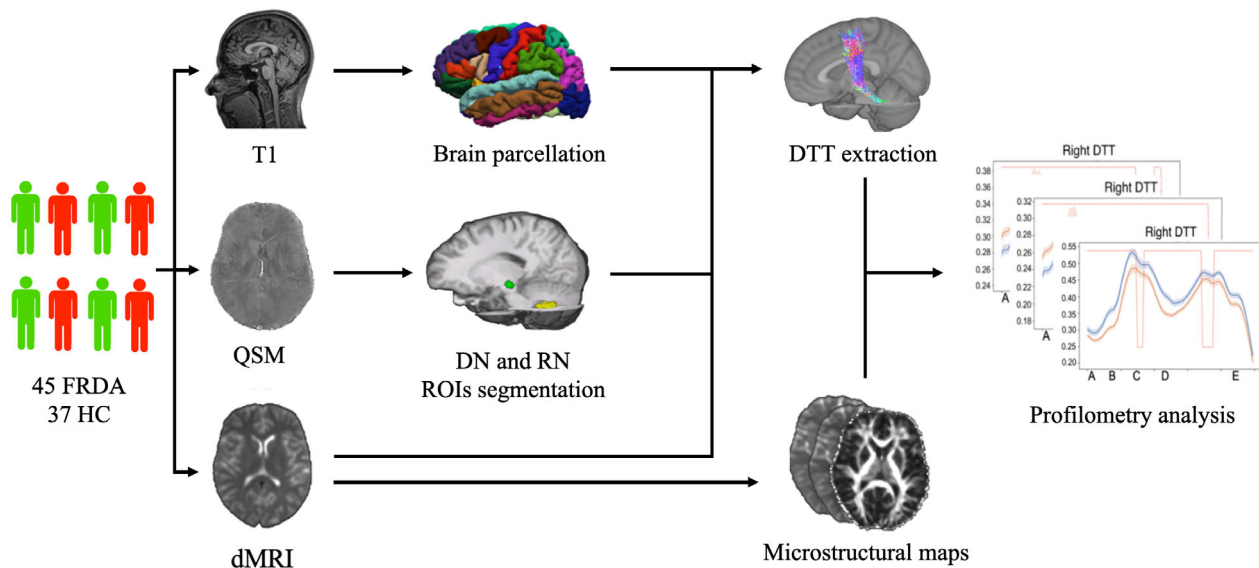


Figure 1. A graphical representation of the main MRI processing steps performed in this study. dMRI, diffusion MRI; DN, dentate nuclei; DTT, dentate-thalamo-cortical tract; FRDA, Friedreich ataxia; HC, healthy controls; QSM, quantitative susceptibility mapping; RN, red nuclei.

Tract reconstruction

The inherent limitations of tractography algorithms present challenges in accurately reconstructing bundles characterized by complex geometries, such as the DTT. To address this, we devised a strategy involving the creation of a bundle template, which was subsequently aligned within the subject-specific space.

For each HC participant, we conducted DTT reconstruction by defining the seed region as the dentate nucleus mask, inclusion regions as the ipsilateral SCP, contralateral red nucleus, and contralateral thalamus, and target region as the contralateral precentral gyrus. Reconstruction was performed separately for the right and left dentate nucleus seed regions. The reconstructed bundles from each dataset were registered to Montreal Neurological Institute (MNI) standard space and averaged to create a study-specific template.

This template was then subjected to refinement using the *recobundle*²⁴ software, a tool used to filter out streamlines that deviate from the intended bundle geometry. Briefly, the software operates by leveraging an atlas of the same bundle, selectively retaining streamlines that exhibit maximum similarity between the input bundle and the atlas. Since the DTT is not a conventionally explored bundle, an

atlas of this structure was not available. Consequently, we constructed the atlas by retaining tractography streamlines common to at least 50% of the subjects while adhering to the bundle mask. Segments shorter than 12 mm were then excluded and we further augmented and smoothed the streamlines using an in-house tool. Integrating the atlas into the *recobundle* software allowed us to generate a clean template of the DTT, which was then co-registered to each subject's space. An example of the DTTs obtained through our pipeline is presented in Figure 2.

In contrast, the arcuate fasciculus, a frequently studied bundle in similar investigations, was extracted from global tractography using the white matter query language tool²⁵ for each HC participant. To ensure methodological coherence analogous to our approach with the DTT, we created a template for this tract by aligning the reconstructed bundles in MNI standard space and merging them. The resulting template was also subject to a cleaning process using the *recobundle* method. Unlike the DTT case, an atlas was readily available for this process, obviating the need for manual creation.

The selection of the arcuate fasciculus for examination was grounded in the assumption that the FRDA disease process does not elicit spatial variations in the diffusivity properties of this bundle.

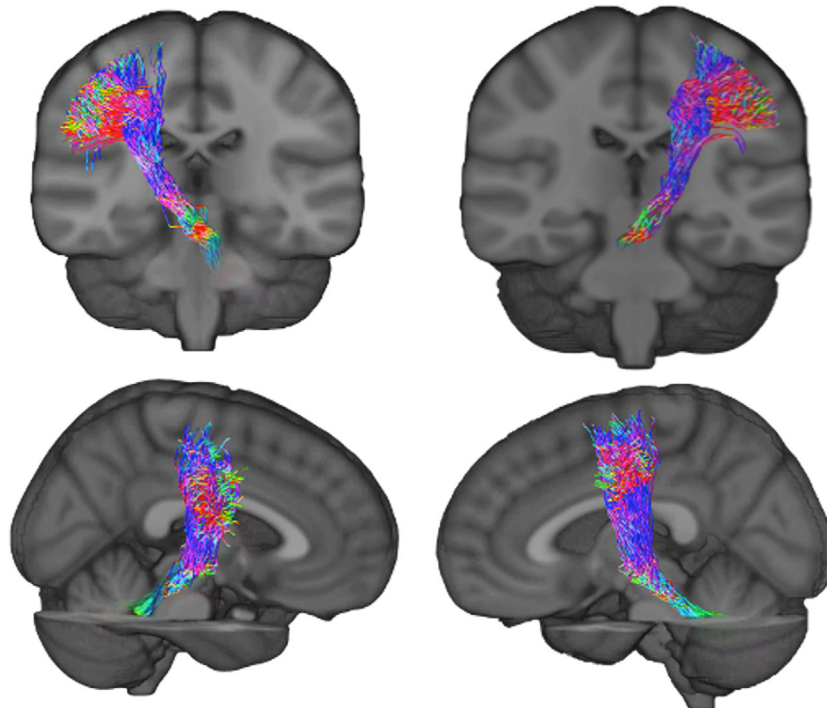


Figure 2. Coronal (upper row) and sagittal (lower row) planes showing an example of the left and right DTT obtained at the end of the dMRI processing steps. DTT, dentate-thalamo-cortical tract; dMRI, diffusion MRI.

Profilometry analysis

To evaluate the degree of involvement of the DTT tract in FRDA, we carried out a profilometric analysis. Currently available profilometry analysis software^{26,27} does not include a standard pipeline for the DTT bundle. Therefore, we modified the tractometry pipeline implemented in the TractSeg²⁸ tool to apply it to this tract. Specifically, as suggested by Chandio and colleagues,²⁶ we sampled the streamlines at 100 equidistant points. We then calculated the centroid of the bundle and assigned the closest point of each streamline to the corresponding centroid point.²⁹ Subsequently, we assigned the value of each microstructural diffusion parameter (FA/MD/RD) in the corresponding voxel with each streamline to the designated centroid point.³⁰ The values at each centroid point were then averaged across groups using functions implemented in dipy (<https://dipy.org/documentation/1.4.1/reference/dipy.stats/#gaussian-weights>). The same procedure was replicated for the arcuate fasciculus. To reduce possible bias in the results arising from different alignment of the dMRI acquisitions (i.e., “pure” axial vs AC-PC orientation), the microstructural values were normalized by the average apparent diffusion coefficient (ADC) of cerebrospinal fluid (CSF) within the ventricles of each subject.

Statistical analysis

A comparison of the mean FA, MD, and RD within each tract³¹ between healthy controls and FRDA patients was first undertaken using linear regression, controlling for age and sex, implemented in R (<https://www.r-project.org/>). Group differences between FRDA and HC along the DTT and arcuate fasciculus were then assessed using

statistical models implemented in TractSeg,²⁸ accounting for age and sex as possible confounding factors. Statistical analysis was performed on the entire pooled group, as well as independently for each site to demonstrate consistency. Results were considered significant for $p < 0.05$ after correction for multiple comparisons.²⁹ Effect size was calculated using Cohen’s d , with values equal to 0.2, 0.5 and higher than 0.8 interpreted as a small, medium or large effect, respectively.³²

Correlations between FA values (as a global index of microstructural involvement of the bundle) and the SARA scale (disease severity), age at onset and mean GAA length³³ were also tested both evaluating the mean FA value along the entire tract (via partial correlation analysis) and using a profilometry approach via TractSeg and its “target” option²⁸, both corrected for age and sex. Given the exploratory nature of these last analyses, results are reported at $p < 0.05$ without correction for multiple comparisons.

Results

Significant between-group differences in all three microstructural diffusion properties were evident in the DTT when assessed globally (i.e., mean values across the entirety of the tract). A mean decrease in FA and mean increases in MD and RD were evident in the FRDA cohort relative to controls (all comparisons $p < 0.001$ and $R^2 \leq 0.49$) (Table 2). The direction of these effects was as expected, with each representing a loss of microstructural integrity in the FRDA cohort.

The profilometry analysis showed widespread abnormalities in all three metrics across the length of the DTT (Fig. 3; minimum $p < 1 \times 10^{-12}$, $< 1 \times 10^{-8}$ and $< 1 \times 10^{-11}$, for FA, MD and RD respectively, all $d \geq 1.3$).

Table 2. Results of the mean tract profiles analysis.

	FA	MD $\times 10^{-3}$ mm ² /s	RD $\times 10^{-3}$ mm ² /s
Left DTT	FRDA: 0.37 \pm 0.02	FRDA: 0.84 \pm 0.05	FRDA: 0.67 \pm 0.05
	HC: 0.40 \pm 0.02	HC: 0.78 \pm 0.03	HC: 0.61 \pm 0.03
	p -value < 0.001 , $R^2 = 0.53$	p -value < 0.001 , $R^2 = 0.46$	p -value < 0.001 , $R^2 = 0.53$
Right DTT	FRDA: 0.36 \pm 0.02	FRDA: 0.83 \pm 0.03	FRDA: 0.67 \pm 0.04
	HC: 0.39 \pm 0.02	HC: 0.79 \pm 0.03	HC: 0.62 \pm 0.03
	p -value < 0.001 , $R^2 = 0.60$	p -value < 0.001 , $R^2 = 0.49$	p -value 0.001, $R^2 = 0.58$
Left AF	FRDA: 0.38 \pm 0.02	FRDA: 0.75 \pm 0.03	FRDA: 0.60 \pm 0.03
	HC: 0.40 \pm 0.02	HC: 0.73 \pm 0.02	HC: 0.57 \pm 0.02
	p -value < 0.001 , $R^2 = 0.25$	p -value < 0.001 , $R^2 = 0.22$	p -value < 0.001 , $R^2 = 0.26$
Right AF	FRDA: 0.34 \pm 0.02	FRDA: 0.77 \pm 0.03	FRDA: 0.63 \pm 0.04
	HC: 0.35 \pm 0.02	HC: 0.74 \pm 0.02	HC: 0.60 \pm 0.03
	p -value < 0.001 , $R^2 = 0.19$	p -value < 0.001 , $R^2 = 0.27$	p -value < 0.001 , $R^2 = 0.29$

Table summarizing the results of the between-group mean tract profiles analysis. MD and RD are expressed in 10^{-3} mm²/s.

AF, arcuate fasciculus; DTT, dentate-thalamo-cortical tract; FA, fractional anisotropy; FRDA, Friedreich ataxia; HC, healthy controls; MD, mean diffusivity; RD, radial diffusivity.

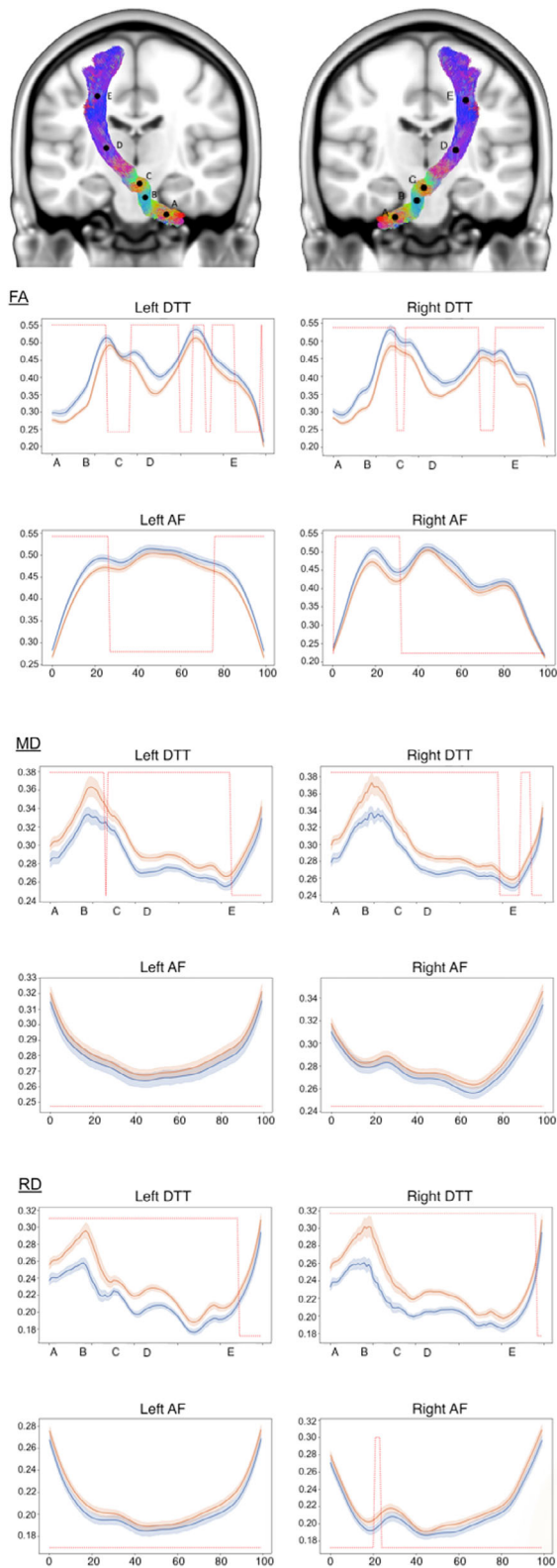


Figure 3. Results of the profilometry analysis of the DTT in FRDA. In the first row, superimposed on a standard brain atlas, the template of the DTT is shown along with its five anatomical inclusion regions (A: DN; B: SCP; C: RN; D: thalamus; E: precentral gyrus). In the lowest rows, results of the profilometry analysis, for both the DTT and AF (used as control region), of the microstructural maps here investigated. Orange and blue lines represent individuals with FRDA and HC, respectively. Red lines indicate significant differences between groups at that level. AF, arcuate fasciculus; DN, dentate nuclei; DTT, dentate-thalamo-cortical tract; FA, fractional anisotropy; FRDA, Friedreich ataxia; HC, healthy controls; MD, mean diffusivity; RD, radial diffusivity; RN, red nuclei; SCP, superior cerebellar peduncle.

The microstructural abnormalities were most pronounced in the first part of the tract, particularly between the dentate nuclei and red nuclei, as well as adjacent to the thalamus (Fig. 3). No differences were readily evident between the right and the left tracts (Fig. 3). Stratification of the analysis by site showed a similar pattern of microstructural damage for all three sites (Fig. S1). A graphical representation of the localization and the degree of microstructural damage affecting the DTT according to the cohen-d values is shown in Figure 4, with the corresponding plot that is available in Figure S2.

For the arcuate fasciculus, individuals with FRDA also showed significant average microstructural damage of the entire bundle for the three tested metrics relative to controls, although with much smaller effect sizes than in the DTT (all comparisons $p < 0.001$ and $R^2 \leq 0.19$) (Table 2). Conversely, however, the profilometry analysis did not show a pattern of more pronounced damage in a specific portion of the bundle, with the exception of small group differences in FA at the beginning and the end of the fascicle (Fig. 3).

The exploratory analysis of associations between microstructural damage of the DTT and the clinical status of individuals with FRDA patients revealed a correlation between GAA triplets length and mean FA values of the DTT (left: $\rho = -0.41$, $p = 0.007$; right: $\rho = -0.39$, $p = 0.01$), while no other correlations with the remaining clinical variables were found (all p values > 0.29) (Fig. 5). Interestingly, when a profilometry approach was performed, a bilateral negative correlation between FA values and SARA score at the level of the thalamus (left: $\rho = -0.32$, $p = 0.03$; right: $\rho = -0.34$, $p = 0.02$) emerged, along with a widespread association to mean GAA length (left: $\rho = -0.45$, $p = 0.002$; right: $\rho = -0.44$, $p = 0.003$) (Fig. 6). Finally, no correlations between AAO and DTT microstructure were found, with the exception of a small cluster of correlation at the level of the left corona radiata ($\rho = 0.38$, $p = 0.01$).

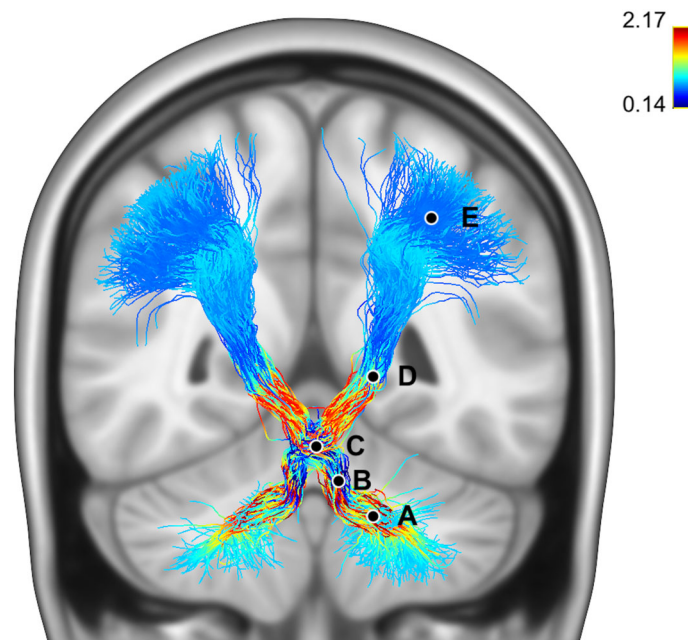


Figure 4. Representation of the spatial profile and magnitude of microstructural damage affecting the DTT (along with its five anatomical inclusion regions—A: DN; B: SCP; C: RN; D: thalamus; E: precentral gyrus) using a color-coded scale weighted by Cohen-d values. DN, dentate nuclei; DTT, dentate-thalamo-cortical tract; RN, red nuclei; SCP, superior cerebellar peduncle.

Discussion

In FRDA, the current literature offers evidence of a gradient of CNS damage in which changes occur earliest and are most pronounced in the spinal cord and the dentate nucleus—the putative regions of primary CNS pathology in this disorder—and occur later and are less robust toward the cerebral cortex. This evidence supports the likelihood of transsynaptic damage ascending from the spinal cord and cerebellum to the cerebrum. Here, we corroborate this evidence by demonstrating a complex pattern of microstructural damage affecting the cerebellar-cerebral pathways, most pronounced in the dentato-thalamic sections of the tracts (with some notable effects at the level of the SCP) compared with the thalamo-cortical portions, suggesting a complex, non-linear but decreasing gradient of damage ascending from the DN to the motor cortex.

Our finding of an ascending gradient of pathology affecting the DTT in FRDA is in line with other neurodegenerative features of this disease.^{11,17,34} In particular, volumetric MRI findings indicate that cerebellar, brainstem, and spinal changes occur early in the course of the disease, while tissue loss in the cerebrum only becomes apparent in more late-stages.^{11,34} Similarly, atrophy of the dorsal root ganglia, which give rise to the ascending sensory spinal tracts, are also early and core features of the disease. It has been hypothesized that the dorsal root

ganglia changes have direct anterograde effects on both the dorsal and the Clarke columns in the spinal cord,¹⁷ impacting the dorsal spinocerebellar tract, which innervates the cerebellar cortex, and in turn, the dentate nuclei. This may provide an additional mechanism of secondary cerebellar atrophy and DTT degeneration in addition to anterograde (and perhaps retrograde) damage resulting from dentate nucleus pathology.

Our results also highlight the importance of avoiding, where possible, the use of mean values along the entire DTT when analyzing dMRI experimental data in FRDA studies. Although mean values can provide useful disease insights, as demonstrated by previous research in FRDA^{35–37} and other conditions defined by diffuse white matter damage,³⁸ subtleties in the anatomical profile may be hidden by such an analysis. The profilometry approach applied here points to a more nuanced spatial pattern of microstructural damage in the DTT in individuals with FRDA. In particular, not only is the tract more impacted proximal to the dentate nucleus, but there also appears to be a relatively targeted change in FA values in the region of the thalamus. This information provides a more detailed understanding of neuroanatomical disease expression, while also offering the potential to identify more sensitive biomarkers that may be relevant for disease tracking and treatment monitoring. Furthermore, we speculate that this approach might also represent a useful tool also for the investigation of other forms of ataxia,

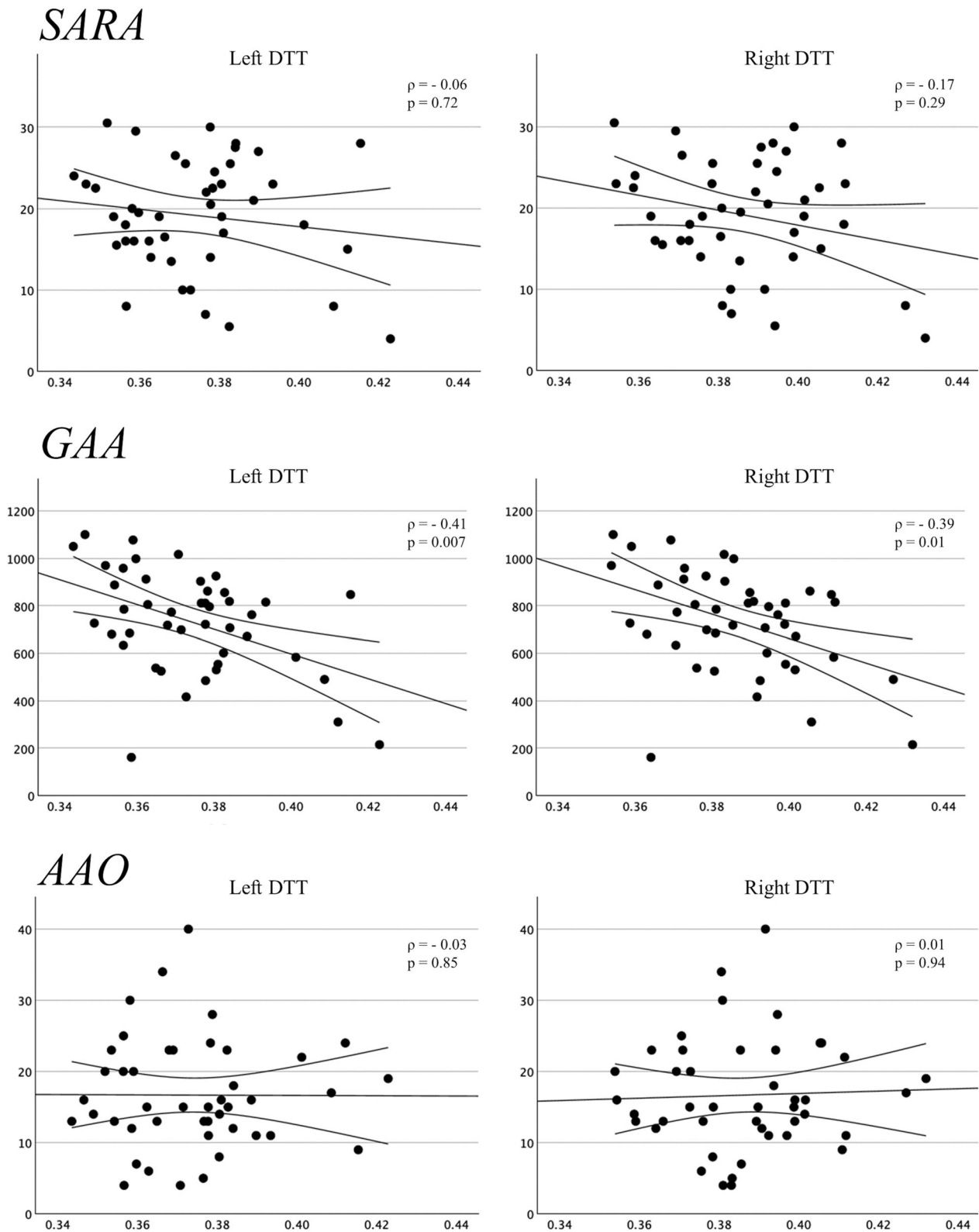


Figure 5. Results of the correlation analyses between mean FA value (x-axes) along the entire DTT and SARA scores, mean GAA length and AAO (y-axes). AAO, age at onset; DTT, dentate-thalamo-cortical tract; FA, fractional anisotropy; SARA, scale for the assessment and rating of ataxia.

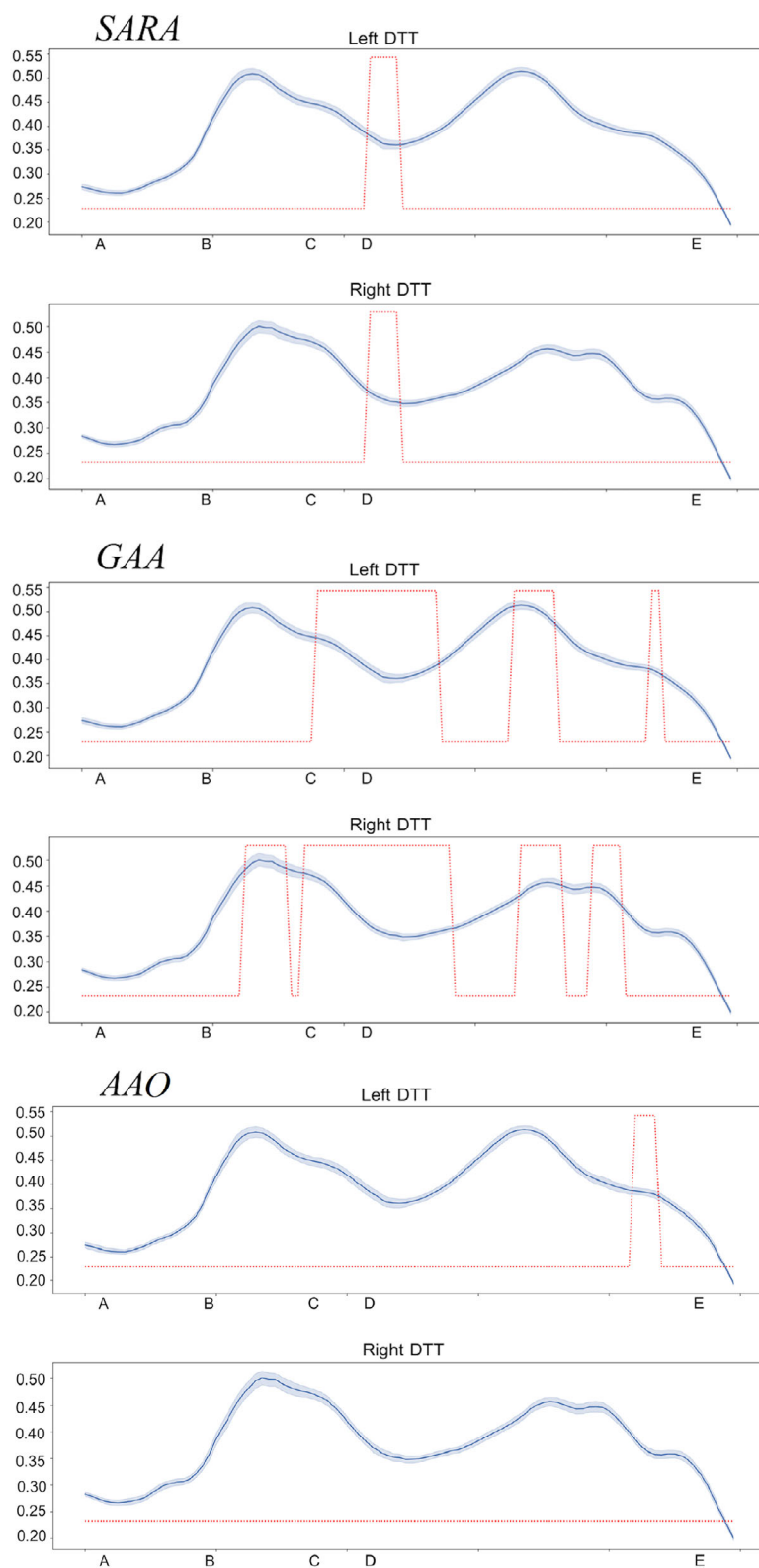


Figure 6. Results of the correlation analyses using a profilometry approach between FA values (y-axes) along the DTT (x-axis) and SARA scores, mean GAA length and AAO). Red lines indicate where, along the DTT, significant correlations between the microstructural damage and the corresponding clinical variable occur. AAO, age at onset; DTT, dentate-thalamo-cortical tract; FA, fractional anisotropy; SARA, scale for the assessment and rating of ataxia.

including spinocerebellar ataxias, where microstructural changes of cerebellar efferences through the SCP have been reported.^{39–41}

Finally, although AD changes have been reported in FRDA, the evaluation of this dMRI metric was not included in this work as the direction of “axial” diffusivity is not consistently maintained in pathological tissue, and furthermore it is not always aligned with the underlying tissue architecture. This discrepancy is particularly significant in regions with low anisotropy, in voxels affected by partial volume, and in areas where crossing fibers are present and comparing eigenvalues between different groups of subjects may simply indicate differences in the underlying tissue structure, unrelated to the pathology.^{42–44}

Although exploratory, our analysis also supports the clinical relevance of the observed microstructural changes of the DTT in FRDA. In particular, we found a relatively widespread correlation between GAA length and microstructural integrity along the DTT, with a more profound effect at the level of the thalami. Furthermore, greater ataxia severity (measured via SARA) was associated with greater microstructural damage at the level of the thalamic synapse, a result hindered by the global microstructural correlation analysis, similar to the triplets’ finding and mirroring the observed increase in the FRDA vs. control between-group difference in this region. Somewhat unexpectedly, however, this correlation was not evident in DTT regions close to the dentate nucleus, where the between-group difference was also pronounced. This pattern suggests a hypothesis that pathology at the level of the thalamic synapse, where the first axon of the DTT terminates, may contribute more to cerebellar-cerebral dysfunction and behavioral outcomes in FRDA than axonal degeneration or demyelination.^{6,9,10,38} However, this speculation needs to be interpreted cautiously, and confirmed by future multicentric prospective studies with standardized clinical and MRI protocols.

A limitation of the present study is that although robust efforts have been made to harmonize the data, and the analysis conducted independently for each different site showed three similar patterns of damage (thus reducing the possibility of possible bias inducted by the processing steps), the dMRI data were acquired on different scanners and with different protocols. For this reason, we were not able to apply more advanced methods of data analysis, such as neurite orientation dispersion and density imaging (NODDI), to investigate more subtle neurodegenerative involvement of the DTT in FRDA.

In summary, our study further expands the current knowledge about brain involvement in FRDA and shows the presence of significant microstructural abnormalities at the level of the main cerebellar efference in these individuals. These findings are in line with the hypothesis of

an anterograde secondary degeneration arising from the dentate nuclei to the primary motor cortex, suggesting the possibility of employing dMRI and profilometry to longitudinally evaluate damage spread and treatment response in FRDA.

Author Contributions

Sirio Coccozza: Conceptualization, Investigation, Formal analysis, Writing – original draft. **Sara Bosticardo:** Conceptualization, Data curation, Formal analysis, Writing – review & editing. **Matteo Battocchio:** Data curation, Investigation, Writing – review & editing. **Louise Corben:** Data curation, Writing – review & editing. **Martin Delatycki:** Data curation, Writing – review & editing. **Gary Egan:** Data curation, Writing – review & editing. **Nellie Georgiou-Karistianis:** Data curation, Writing – review & editing. **Serena Monti:** Supervision, Writing – review & editing. **Giuseppe Palma:** Data curation, Writing – review & editing. **Chiara Pane:** Supervision, Writing – review & editing. **Francesco Saccà:** Supervision, Writing – review & editing. **Simona Schiavi:** Supervision, Writing – review & editing. **Louisa Selvadurai:** Supervision, Writing – review & editing. **Mario Tranfa:** Supervision, Writing – review & editing. **Alessandro Daducci:** Conceptualization, Supervision, Writing – review & editing. **Arturo Brunetti:** Conceptualization, Supervision, Writing – review & editing. **Ian H. Harding:** Conceptualization, Methodology, Supervision, Writing – review & editing.

Acknowledgments

We thank the study participants.

Funding Information

This research received no specific grant from any funding agency in the public, commercial, or not-for-profit sectors.

Conflict of Interest

Sirio Coccozza has served on scientific Advisory Board for Amicus Therapeutics and has received Grants from FISM and Telethon. The remaining authors have nothing to disclose.

References

1. Campuzano V, Montermini L, Moltò MD, et al. Friedreich’s ataxia: autosomal recessive disease caused by an intronic GAA triplet repeat expansion. *Science*. 1996;271(5254):1423–1427.

2. Pandolfo M, Manto M. Cerebellar and afferent ataxias. *Continuum*. 2013;19:1312-1343.
3. Deistung A, Jäschke D, Draganova R, et al. Quantitative susceptibility mapping reveals alterations of dentate nuclei in common types of degenerative cerebellar ataxias. *Brain Commun*. 2022;4(1):fcab306.
4. Ward PGD, Harding IH, Close TG, et al. Longitudinal evaluation of iron concentration and atrophy in the dentate nuclei in Friedreich ataxia. *Mov Disord*. 2019;34(3):335-343.
5. Stefanescu MR, Dohnalek M, Maderwald S, et al. Structural and functional MRI abnormalities of cerebellar cortex and nuclei in SCA3, SCA6 and Friedreich's ataxia. *Brain*. 2015;138(5):1182-1197.
6. Rezende TJR, Martinez ARM, Faber I, et al. Developmental and neurodegenerative damage in Friedreich's ataxia. *Eur J Neurol*. 2019;26(3):483-489.
7. Coccozza S, Costabile T, Pontillo G, et al. Cerebellum and cognition in Friedreich ataxia: a voxel-based morphometry and volumetric MRI study. *J Neurol*. 2020;267(2):350-358.
8. Selvadurai LP, Harding IH, Corben LA, et al. Cerebral and cerebellar grey matter atrophy in Friedreich ataxia: the IMAGE-FRDA study. *J Neurol*. 2016;263(11):2215-2223.
9. Vavla M, Arrigoni F, Nordio A, et al. Functional and structural brain damage in Friedreich's ataxia. *Front Neurol*. 2018;9:747.
10. Selvadurai LP, Corben LA, Delatycki MB, et al. Multiple mechanisms underpin cerebral and cerebellar white matter deficits in Friedreich ataxia: the IMAGE-FRDA study. *Hum Brain Mapp*. 2020;41(7):1920-1933.
11. Harding IH, Chopra S, Arrigoni F, et al. Brain structure and degeneration staging in Friedreich ataxia: magnetic resonance imaging volumetrics from the ENIGMA-Ataxia Working Group. *Ann Neurol*. 2021;90(4):570-583.
12. Dogan I, Romanzetti S, Didszun C, et al. Structural characteristics of the central nervous system in Friedreich ataxia: an in vivo spinal cord and brain MRI study. *J Neurol Neurosurg Psychiatry*. 2019;90(5):615-617.
13. Akhlaghi H, Yu J, Corben L, et al. Cognitive deficits in Friedreich ataxia correlate with micro-structural changes in Dentatorubral tract. *Cerebellum*. 2014;13(2):187-198.
14. Zalesky A, Akhlaghi H, Corben LA, et al. Cerebello-cerebral connectivity deficits in Friedreich ataxia. *Brain Struct Funct*. 2014;219(3):969-981.
15. Coccozza S, Costabile T, Tedeschi E, et al. Cognitive and functional connectivity alterations in Friedreich's ataxia. *Ann Clin Transl Neurol*. 2018;5(6):677-686.
16. Kerestes R, Cummins H, Georgiou-Karistianis N, et al. Reduced cerebello-cerebral functional connectivity correlates with disease severity and impaired white matter integrity in Friedreich ataxia. *J Neurol*. 2023;270:2360-2369. doi:10.1007/s00415-023-11637-x
17. Koeppe AH. Friedreich's ataxia: pathology, pathogenesis, and molecular genetics. *J Neurol Sci*. 2011;303(1-2):1-12.
18. Smith RE, Tournier J-D, Calamante F, Connelly A. Anatomically-constrained tractography: improved diffusion MRI streamlines tractography through effective use of anatomical information. *NeuroImage*. 2012;62(3):1924-1938.
19. Jenkinson M, Smith S. A global optimisation method for robust affine registration of brain images. *Med Image Anal*. 2001;5(2):143-156.
20. Jeurissen B, Tournier J-D, Dhollander T, Connelly A, Sijbers J. Multi-tissue constrained spherical deconvolution for improved analysis of multi-shell diffusion MRI data. *NeuroImage*. 2014;103:411-426.
21. Tournier JD, Calamante F, Connelly A. Improved probabilistic streamlines tractography by 2nd order integration over fibre orientation distributions. *Proc Int Soc Magn Reson Med*. 2010;1670.
22. Le Bihan D, Mangin J-F, Poupon C, et al. Diffusion tensor imaging: concepts and applications. *J Magn Reson Imaging*. 2001;13(4):534-546.
23. Fortin J-P, Parker D, Tunç B, et al. Harmonization of multi-site diffusion tensor imaging data. *NeuroImage*. 2017;161:149-170.
24. Garyfallidis E, Côté M-A, Rheault F, et al. Recognition of white matter bundles using local and global streamline-based registration and clustering. *NeuroImage*. 2018;170:283-295.
25. Wassermann D, Makris N, Rathi Y, et al. The white matter query language: a novel approach for describing human white matter anatomy. *Brain Struct Funct*. 2016;221(9):4705-4721.
26. Chandio BQ, Risacher SL, Pestilli F, et al. Bundle analytics, a computational framework for investigating the shapes and profiles of brain pathways across populations. *Sci Rep*. 2020;10(1):17149.
27. Dayan M, Monohan E, Pandya S, et al. Profilometry: a new statistical framework for the characterization of white matter pathways, with application to multiple sclerosis. *Hum Brain Mapp*. 2016;37(3):989-1004.
28. Wasserthal J, Maier-Hein KH, Neher PF, et al. Multiparametric mapping of white matter microstructure in catatonia. *Neuropsychopharmacology*. 2020;45(10):1750-1757.
29. Yeatman JD, Dougherty RF, Myall NJ, Wandell BA, Feldman HM. Tract profiles of white matter properties: automating fiber-tract quantification. *PLoS One*. 2012;7(11):e49790.
30. Tournier J-D, Smith R, Raffelt D, et al. MRtrix3: a fast, flexible and open software framework for medical image processing and visualisation. *NeuroImage*. 2019;202:116137.
31. Kruper J, Yeatman JD, Richie-Halford A, et al. Evaluating the reliability of human brain white matter tractometry. *Aperture Neuro*. 2021;2021(1):25.
32. Sullivan GM, Feinn R. Using effect size—or why the *p* value is not enough. *J Grad Med Educ*. 2012;4(3):279-282.

33. Filla A, De Michele G, Cavalcanti F, et al. The relationship between trinucleotide (GAA) repeat length and clinical features in Friedreich ataxia. *Am J Hum Genet.* 1996;59(3):554-560.
34. Selvadurai LP, Georgiou-Karistianis N, Shishegar R, et al. Longitudinal structural brain changes in Friedreich ataxia depend on disease severity: the IMAGE-FRDA study. *J Neurol.* 2021;268(11):4178-4189.
35. Della Nave R, Ginestroni A, Tessa C, et al. Brain white matter tracts degeneration in Friedreich ataxia. An in vivo MRI study using tract-based spatial statistics and voxel-based morphometry. *NeuroImage.* 2008;40(1):19-25.
36. Vieira Karuta SC, Raskin S, De Carvalho NA, et al. Diffusion tensor imaging and tract-based spatial statistics analysis in Friedreich's ataxia patients. *Parkinsonism Relat Disord.* 2015;21(5):504-508.
37. Rizzo G, Tonon C, Valentino ML, et al. Brain diffusion-weighted imaging in Friedreich's ataxia: DWI in FRDA. *Mov Disord.* 2011;26(4):705-712.
38. Bells S, Cercignani M, Deoni S, et al. Tractometry-comprehensive multi-modal quantitative assessment of white matter along specific tracts. *Proc Int Soc Magn Reson Med.* 2011;678.
39. Mandelli ML, De Simone T, Minati L, et al. Diffusion tensor imaging of spinocerebellar ataxias types 1 and 2. *Am J Neuroradiol.* 2007;28(10):1996-2000.
40. Park YW, Joers JM, Guo B, et al. Assessment of cerebral and cerebellar white matter microstructure in spinocerebellar ataxias 1, 2, 3, and 6 using diffusion MRI. *Front Neurol.* 2020;11:411.
41. Ying SH, Landman BA, Chowdhury S, et al. Orthogonal diffusion-weighted MRI measures distinguish region-specific degeneration in cerebellar ataxia subtypes. *J Neurol.* 2009;256(11):1939-1942.
42. You Y, Joseph C, Wang C, et al. Demyelination precedes axonal loss in the transneuronal spread of human neurodegenerative disease. *Brain.* 2019;142(2):426-442.
43. Schiavi S, Petracca M, Sun P, et al. Non-invasive quantification of inflammation, axonal and myelin injury in multiple sclerosis. *Brain.* 2021;144(1):213-223.
44. Wheeler-Kingshott CAM, Cercignani M. About "axial" and "radial" diffusivities. *Magn Reson Med.* 2009;61(5):1255-1260.

Supporting Information

Additional supporting information may be found online in the Supporting Information section at the end of the article.

Figure S1.

Figure S2.

Data S1.